Autonomous Dual Active Power-frequency Control in Power System with Small-scale Photovoltaic Power Generation

Noha Harag, Masaki Imanaka, *Member*, *IEEE*, Muneaki Kurimoto, *Member*, *IEEE*, Shigeyuki Sugimoto, *Member*, *IEEE*, Hassan Bevrani, *Senior Member*, *IEEE*, and Takeyoshi Kato, *Member*, *IEEE*

***Abstract*—Active power control of the photovoltaic (PV) power generation system is a promising solution to regulate frequency fluctuation in a power system with high penetration of renewable energy. This paper proposes an autonomous active power control of a small-scale PV system for supporting the inertial response of synchronous generators and power-frequency control. In the proposed control approach, an effective grid frequency regulation scheme is realized using slow- and fast-frequency responses. A low-pass filter based frequency measurement is used for slow-frequency response, while direct frequency measurement is used for fast-frequency response. The designed dual droop characteristic-based control is shaped to achieve a smooth transition between slow- and fast-frequency responses. The performance of the proposed control approach is demonstrated for serious disturbance scenarios, i.e., considerable power-load imbalance and generation trip. In the power-load imbalance test scenario, the proposed control approach works properly within the normal frequency deviation region even when the frequency deviation exceeds that region occasionally. In the generation trip test, the frequency deviation is mitigated quickly, and the employed droop control is smoothly transferred from the slow- to fast-frequency responses.**

***Index Terms*—Dual droop control, fast-frequency response, slow-frequency response, inertial response, power-frequency control, regulation support.**

I. Introduction

THE increased penetration of photovoltaic (PV) power leads to various challenges for the stable operation of the power system. For example, utilizing PV power to maintain the demand-supply balance in the daytime with a high power supply of PV is a challenging issue. The flexibility of renewable energy systems (RESs) for maintaining grid frequency should be increased. PV systems currently undergo the maximum power point tracking (MPPT) control in different techniques [1]-[3] because of its unstable power output property. This property depends on irradiance variation which increases the fluctuation of the residual power load in the overall power system. Despite the increased fluctuation, the high penetration of PV systems leads to less contribution of the conventional thermal power plants in the overall power generation, hence their ability to regulate the power will also be reduced.

The power output curtailment is currently applied to maintain the balance between supply and demand when a high-power supply of PV is predicted. The curtailment can be a valuable resource, supporting grid control and improving system flexibility. It can also be used to allow PV systems to generate at reduced levels so that it can ramp up quickly to balance the system [4]. The amount of curtailed power, duration, and method of curtailment are discussed through examples of several countries that apply this process in different manners [5]. Power curtailment is crucial for the installation of different scales of PV systems. For example, in [6], large-scale integration of PV power in a distribution grid signifies the application of power curtailment in controlling voltage, feeder currents, distribution substation overloading and the grid frequency. Moreover, based on the real power curtailment of inverters, [7] proposes a strategy to enhance the performance of significantly unbalanced low-voltage (LV) distribution networks with high penetration of residential PV.

Although the curtailment has proved its ability in supporting the frequency through different methods, more flexibilities in active power control (APC) strategies are required by PV systems to support the grid frequency regulation in all time frames as discussed in several studies [8]-[10].

During normal frequency deviation due to small disturbances in load or generation, the APC in the grid is an essential issue [11]. The frequency has to be handled within a certain range. The response to this scenario will take place by generating units with automatic generation control (AGC) when they respond to different regulation timescales [12]. The load following controls tend to be slow in response. Additionally, these controls can either be manually or automatically set. Modern inverter-interfaced PV generators can re-

Manuscript received: September 23, 2020; revised: January 27, 2021; accepted: April 8, 2021. Date of CrossCheck: April 8, 2021. Date of online publication: June 22, 2021.

N. Harag (corresponding author) is with the Electrical Engineering Department of Nagoya University, Nagoya, Japan (e-mail: harag.noha.mamdouh.ali.hassan@a.mbox.nagoya-u.ac.jp).

H. Bevrani is with University of Kurdistan, Sanandaj, Iran (e-mail: bevrani@uok.ac.ir).

M. Imanaka, M. Kurimoto, S. Shigeyuki, and T. Kato are with the Institute of Materials and Systems for Sustainability of Nagoya University, Nagoya, Japan (e-mail: imanaka@imass.nagoya-u.ac.jp; kurimoto@nuee.nagoya-u.ac.jp; sugimoto.shigeyuki@chuden.co.jp; tkato@nuee.nagoya-u.ac.jp).

DOI: 10.35833/MPCE.2020.000700

spond similarly, i.e., they can provide these various forms of APC in time frames even faster than conventional generators [13].

RESs have improved frequency control using fast-frequency response based on a generic system frequency response (GSFR) [14]. Wind turbines have also showed the applicability of the fast-frequency impact of curtailment response control. For example, when a fast primary frequency regulation mechanism is activated in a wind power system, the frequency response is highly enhanced [15]. The participation of wind power in primary frequency regulation by its reserved capacity is discussed in [16]-[18].

Compared with fast-frequency response control of wind power, fewer contributions to fast-frequency response control schemes by PV inverters are made. Among these control schemes, simultaneous fast-frequency response control and power oscillation damping control are performed using large-scale PV plants controlled by STATCOM to enhance frequency regulation and small-signal stability of power systems [19]. The feasibility of providing fast-frequency response control by PV plant has also been demonstrated on a 300 MW PV plant in California, USA [20]. However, these studies only focus on large-scale PV systems.

Some studies represent active power-frequency (p-f) droop control, providing fast-frequency response by PV inverters. For instance, [21] focuses on providing frequency reserve using autonomous *p-f* functions that modify active power according to the measured grid frequency. Reference [21] discusses the design of the *p-f* curve for the curtailment, dead band, and droop setting, hence the performance of different penetrations of PV is tested along with the aforementioned parameters during contingencies. Another strategy of power adjustment and frequency regulation is stated in [22] where two control designs are created: a frequency droop control mode for PV that provides primary frequency support to power systems and an emergency control mode that prevents system frequency collapse. Also, a predictive PV inverter control method for fast and accurate control of active power is represented in [23]. The rapid APC (RAPC) method implemented on PV inverter increases the effectiveness of various higher-level controls designed to mitigate grid frequency contingency events, including fast *p-f* droop, inertia emulation, and fast-frequency response, without the need for energy storage. Moreover, [24] investigates the use of grid support functions to improve grid frequency response using a frequency-watt (FW) function for an islanded grid. The approach dampens frequency disturbances associated with variable irradiance conditions as well as contingency events without utilizing expensive energy storage systems or supplemental generation. These studies confirm the importance of *p-f* droop control of PV to regulate frequency during contingencies, yet they lack *p-f* droop control designed to mitigate normal frequency deviations caused by frequent disturbances in load or generation.

To improve the contribution of PV systems to the grid frequency regulation and a further increase of PV active power penetration, it would be more effective to perform a combination of different control schemes in a single PV-based control synthesis problem. In particular, the PV system can accommodate two control schemes. The first is to mitigate frequency deviations in contingencies, and the second is to suppress frequent fluctuations of load or generation disturbances. Most importantly, both control schemes should be applied without affecting each other negatively.

A power system operator can fully control different capacities of PV power output. For a further contribution of whole PV systems, the control should be provided not only by large-scale PV systems but also by medium- and small-scale PV systems. Recently, the number of installed small-scale PV systems in urban areas increases along with the growth of the global PV market. Moreover, PV installations are relatively simple and low in cost for urban areas [25]-[27]. Increased PV installations lead to less dependence on the operator to provide control signals to adjust the magnitude of their response to disturbances. And this independence causes a more efficient and economical operation of the power system [28]. Therefore, active power should be adjusted autonomously by an effective control scheme in response to the frequency deviation in renewable-integrated power systems.

To realize such an APC of PV systems and contribute to both fast- and slow-frequency responses in a power system, this paper proposes an autonomous APC based on a dual *p-f* droop control which can change the droop characteristics depending on the magnitude of frequency change. The objective of this paper is to propose an effective control of the PV system to respond to both slow- and fast-frequency fluctuations. It is shown that both control loops properly work without a negative dynamic conflict.

In this paper, two simulation tests are conducted to examine the proposed control approach. Using a simplified version of the AGC30 model [29], the first test will involve the load-generation imbalance and the second one will simulate the problem of generation dropout. Each test will examine the performance of PV systems with the proposed control as a simple and effective control scheme.

The rest of this paper is organized as follows. Section II presents the initial proposal of APC for supporting grid frequency. Section III presents the enhanced proposal of APC for supporting grid frequency. Section IV presents the summary of dual *p-f* droop methods. Sections V and VI present the power supply-demand balancing for slow- and fast-frequency responses, respectively. This paper is concluded in Section VII.

II. Initial Proposal of APC for Supporting Grid Frequency

The proposed control is based on switching between different droop characteristics according to the magnitude of frequency deviation. In this paper, a combination of two different droop characteristics for slow- and fast-frequency responses is proposed through two designs, e. g., method 1 which is the first design proposal and method 2 which is the second one.

A. Method 1

Figure 1 shows a dual *p-f* droop control of method 1, where *df* is the measurement of the change of frequency,

which can be either slow-frequency deviation df_{slow} or fast-frequency deviation df_{fast}.

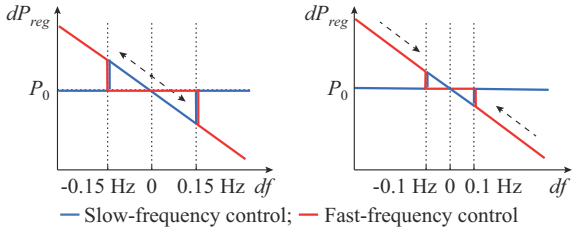

Fig. 1. Dual *p-f* droop control of method 1. (a) *df* is within ±0.15 Hz. (b) *df* passes ±0.15 Hz.

This is a simultaneous combination of two droop characteristics operating in two different modes in terms of frequency deviation separated between small and large frequency deviation ranges determined by the threshold values of $\pm df_{th}$. Based on the measured frequency deviation used in slow-frequency control df_{slow} and fast-frequency control df_{fast}, the corresponding active power change is given as follows.

$$\begin{cases} dP_{slow} = -\dfrac{1}{D}\dfrac{P_{mpp}}{f_0}.df_{slow} \\ dP_{fast} = -\dfrac{1}{D}\dfrac{P_{mpp}}{f_0}.df_{fast} \end{cases} \quad (1)$$

where dP_{slow} and dP_{fast} are the power deviations due to df_{slow} and df_{fast}, respectively; D is the droop setting of 4%; P_{mpp} is the power due to MPPT; and f_0 is the nominal frequency of the power grid, which is 60 Hz in this paper. Although the formulas of dP_{slow} and dP_{fast} are the same, the time-series change in dP_{slow} and dP_{fast} is different because of the difference in measurement method of df_{slow} and df_{fast}.

The proposed control is based on the power output curtailment control, which maintains the pre-set point of active power output P_0 at a lower level than P_{mpp}. The difference between P_{mpp} and P_0 can be utilized as a control reserve for adjusting the active power output according to the fluctuation of the grid frequency.

In the conventional control of PV system, P_{mpp} can be estimated with MPPT control. The proposed control is unable to estimate P_{mpp} on the actual operation point like the conventional MPPT control. Therefore, the proposed control employs *I-V* characteristics for the grid-connected PV system to be controlled, where it observes the short-circuit current I_{sc} and the open-circuit voltage V_{oc}, and estimates P_{mpp} based on the predetermined function formulated with I_{sc} and V_{oc}. A similar method using an additional measurement of solar irradiance is proposed by [13]. I_{sc} in the proposed approach is dominantly dependent on the solar irradiance. Besides, by using V_{oc}, which is dominantly dependent on the module temperature, the estimation of P_{mpp} is expected to be more accurate than the estimation solely by solar irradiance or I_{sc}. The preparation of P_{mpp} data of solar power is further discussed in Section V.

To compare Fig. 1(a) and (b), arrows are added to explain the switch of frequency deviation threshold df_{th} in terms of the direction of frequency deviations. If the direction of actual frequency deviation *df* is increasing (moving outwards), the $\pm df_{th}$ is set to be ±0.15 Hz and if the direction of *df* is decreasing (moving inwards), the $\pm df_{th}$ is set to be ±0.1 Hz. A smaller threshold (±0.1 Hz) is chosen to delay the transition from fast-frequency control to slow-frequency control, i. e., allow the transition to occur at a small frequency deviation.

The switch between frequency thresholds is illustrated in Fig. 2. As the measured frequency increases and crosses ±0.15 Hz, the new threshold becomes ±0.1 Hz. As the measured frequency decreases below ±0.1 Hz, the threshold returns to ±0.15 Hz.

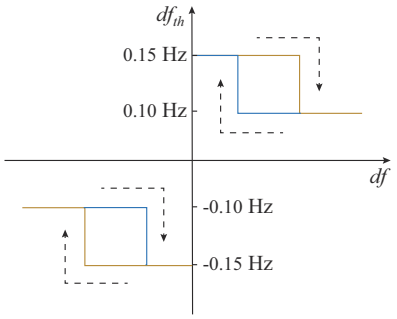

Fig. 2. Change of frequency thresholds in method 1.

The operation of method 1 is explained below and the calculation of total regulation power output dP_{reg} is performed as shown in Fig. 3.

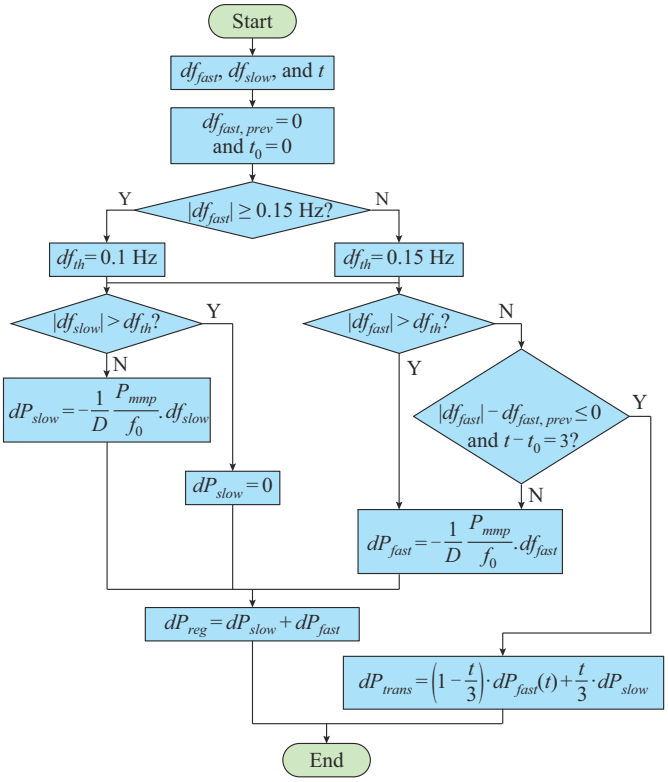

Fig. 3. Flowchart of method 1 of dual *p-f* droop control.

Figure 4 shows the time-series assumption of frequency deviation and the corresponding measurements of frequencies df_{slow} and df_{fast}. *df* is changed to −0.25 Hz at 2 s, recovered to −0.05 Hz at 10 s, and returned to 0 Hz at 20 s. Figure 5 shows the corresponding change in dP_{slow} and dP_{fast}. df_{fast} overlaps *df* due to a small delay of measurement and df_{slow}

follows *df* with about 7 s delay. During such a change in *df*, the slow-frequency control, the fast-frequency control, and the switching from fast to slow work as described below.

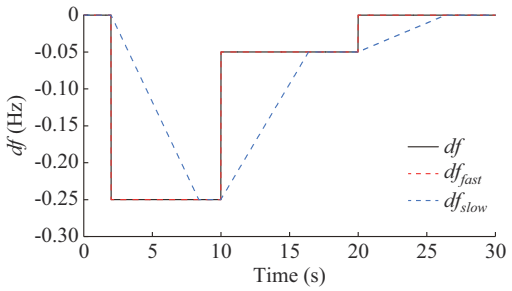

Fig. 4. Time-series assumption of frequency deviation.

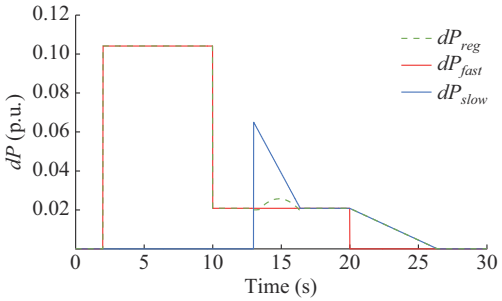

Fig. 5. Time-series operation of dual *p-f* droop control applying method 1.

B. Slow-frequency Control

In the slow-frequency control, the PV system should respond properly to the small-frequency fluctuations, which should be addressed by the LFC in power system. Therefore, the frequency deviation for slow-frequency droop control df_{slow} is calculated based on the observed terminal voltage using several hundred previous cycles through a low-pass filter. In this paper, 400 cycles are used. The frequency measurement df_{slow} slowly follows the system frequency. This measurement will not be as quick as frequency variations which can detect all changes in the system frequency.

We use the slow manner of frequency measurement to activate the slow-frequency control when the frequency deviation is still within the range of ±0.15 Hz. These deviations are caused by the change in electricity demand or power output of other generators. The normal frequency deviation range is reported to be ±0.2 Hz in the power system in Japan [30].

However, in this paper, we select a slightly lower range, i. e., ±0.15 Hz, to suppress all the frequency disturbances within the range and reduce the possibility of its violation beyond the agreed-upon frequency range.

Generally, the frequency thresholds can be decided by the system operator based on the grid code of each region. The frequency threshold divides the region between the normal and abnormal frequency deviations, hence the value of the frequency threshold determines which frequency control operates within or beyond that threshold.

C. Fast-frequency Control

Large frequency fluctuation within a short time span is caused by power plant failures or the disconnection of large loads. In this situation, the immediate activation of fast-frequency response is desirable so as to mitigate the maximum frequency deviation. In the proposed control, the frequency deviation used in the fast-frequency control df_{fast} is calculated based on the observed voltage in the last few cycles. In this paper, 20 cycles are used. The frequency measurement df_{fast} quickly follows the system frequency and it is used to detect any changes in the system frequency.

We use this quick response of frequency measurement to activate the fast-frequency control when the frequency deviation exceeds the range of ±0.15 Hz as shown in Fig. 1. In other words, the droop characteristics of fast-frequency control contain a large dead band to prevent the fast-frequency control when the frequency deviation is small. When the fast-frequency control is activated, the droop setting in the slow-frequency control becomes zero, resulting in no contribution by the slow-frequency control.

The same droop setting is used for both slow- and fast-frequency controls. However, to prevent frequent switching between fast- and slow-frequency controls at ±0.15 Hz, a hysteresis is implemented under the switching condition from fast- to slow-frequency responses as recovery phase. This is done by replacing the droop characteristics of Fig. 1(a) with that of Fig. 1(b). Therefore, in the recovery phase, when the frequency deviation reaches ±0.1 Hz, the APC starts to switch from fast- to slow-frequency response.

D. Switching from Fast- to Slow-frequency Controls

In the case of switching from fast- to slow-frequency controls, the sudden change in power output should be avoided in the recovery phase to normal operation. However, because of the difference between the measured frequency for df_{slow} and df_{fast}, if dP_{slow} is suddenly activated when df_{fast} is below 0.1 Hz and the fast-frequency control is deactivated, there will be a sudden change in dP_{reg}. Note that dP_{slow} is determined by (1) without any limitation (or threshold) as described in Fig. 3, although dP_{slow} is still zero when df_{fast} decreases to ±0.1 Hz in Fig. 1(b).

To reduce the aforementioned sudden change in dP_{reg}, the proposed control approach introduces that the temporal power output dP_{trans} is the power deviation due to transition mode signal as:

$$dP_{trans} = \left(1 - \frac{1}{3}t\right) \cdot dP_{fast} + \frac{1}{3}t \cdot dP_{slow} \tag{2}$$

The total regulation power deviation dP_{reg} is considered as the sum of dP_{fast} and dP_{slow}. However, in the case of recovery, as shown in Fig. 4, when df_{fast} decreases to ±0.1 Hz at 10 s, dP_{slow} calculated with df_{slow} becomes a large value as described above. In this case, if dP_{reg} is still calculated as the sum of dP_{fast} and dP_{slow}, it will lead to a sudden change in dP_{reg}. This can be avoided by changing the addition into a temporal time-variant equation in terms of dP_{fast} and dP_{slow}. And then dP_{reg} will be called dP_{trans} in the transition phase only. Accordingly, dP_{trans} will lead to a smooth transition from fast- to slow-frequency controls without any step increase. Since an equation is created to achieve a smooth transition from fast- to slow-frequency controls, it should

be an equation that has a proportional distribution between dP_{fast} and dP_{slow}. The ratio between dP_{fast} and dP_{slow} keeps changing according to the time of transition t until dP_{trans} shifts gradually from df_{slow} towards dP_{fast}.

III. Enhanced Proposal of APC for Supporting Grid Frequency

Although method 1 seems to be simple as it just switches between the two modes, some complications are observed at the PV regulation power output. These complications include the variations of threshold depending on the measured df_{fast} after switching from slow- to fast-frequency responses and vice versa in the recovery phase. Therefore, a second design is proposed to avoid these complications.

A. Method 2

The combination of the two droop characteristics is expressed in the following manner, where only the slow-frequency response is activated within the threshold value $\pm df_{th}$ and both fast- and slow-frequency responses operate beyond this threshold as shown in Fig. 6. In particular, when df_{fast} exceeds the threshold, dP_{fast} is expressed as a linear equation as stated in (1) while dP_{slow} is expressed with a similar equation but df_{slow} will be equal to df_{th}. Hence, dP_{slow} will be a constant value beyond the threshold. Finally, dP_{reg} will be represented in terms of both dP_{fast} and dP_{slow}. Figure 7 shows the corresponding changes in dP_{slow} and dP_{fast}. During such a change in df, the switching from fast- to slow-frequency responses and vice versa is described in the following subsections.

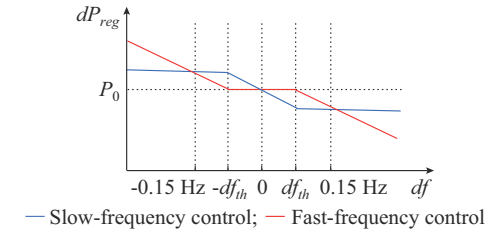

Fig. 6. Dual *p-f* droop control applying method 2.

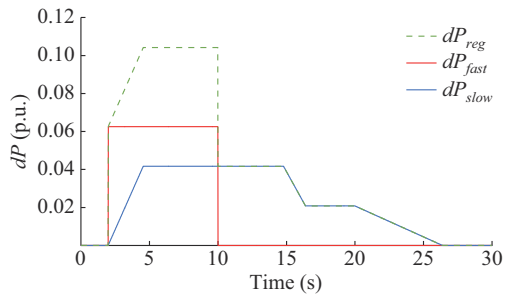

Fig. 7. Time-series operation of enhanced dual *p-f* droop control applying method 2.

B. Switching from Fast- to Slow-frequency Controls

One of the complications involves time settings of t in (2) for transient signal in method 1. To prevent this and provide smooth recovery phase, method 2 has only df_{slow} being activated within the threshold $\pm df_{th}$, and both df_{fast} and df_{slow} are enabled when df_{fast} is more than df_{th}. A transient signal is not necessary since there is no discrete change in the fast- and slow-droop characteristics, and the design of the control scheme becomes simpler than that in method 1.

Besides, Fig. 7 shows time-series operation of enhanced dual *p-f* droop control using method 2. At 10 s, when frequency recovers, dP_{fast} is deactivated immediately, and only slow-frequency control contributes. dP_{reg} does not increase shortly as observed in method 1 because the transient signal is not used in method 2.

C. Switching from Slow- to Fast-frequency Controls

In Fig. 7, both fast- and slow-frequency controls work in correspondence to the frequency fluctuation from 2 s, and the sum of df_{fast} and df_{slow} produces dP_{reg}. However, the response to large frequency deviation becomes slower than method 1 because the slow-frequency is activated even for large frequency fluctuation during abnormal operation. The capability to mitigate the maximum frequency deviation may be lower compared with that of method 1, yet the response time of method 2 is quicker than the conventional generator operation.

As described above, the PV system with dual *p-f* droop control of both method 1 and method 2 is expected to contribute to both frequency controls in a normal situation and fast inertial response in case of severe disturbances. In the following sections, these situations will be tested to conduct a comparison between both methods. Specifically, the interaction between the slow- and fast-dynamic responses in the two methods will be compared. The first simulation test highlights the importance of slow-frequency response in both methods whereas the second test shows the influence of fast response.

IV. Summary of Dual *P-F* Droop Control Methods

Method 1 provides a basic control scheme that combines fast- and slow-frequency droop controls. In literature, fast-frequency droop control is already implemented as discussed in Section I. However, slow-frequency control is preferably added to enhance the droop control in tackling normal disturbances in the power system, and a dual *p-f* droop control can be formed. Method 1 is the initial idea of dual *p-f* droop control because it is simply turning on one frequency control while turning off the other, as the frequency deviation changes. Moreover, it needs an additional control such as transition signal for practical use, resulting in a complicated process of parameter setting. However, method 2 provides a complementary original idea to improve the operation of fast- and slow-frequency controls, i.e., both frequency controls can operate simultaneously. Specifically, it also enhances the behavior of the proposed control when switching between fast- and slow-frequency controls which is the major problem encountered when method 1 is applied. A summary of advantages and disadvantages of both methods is shown in Table I.

TABLE I
SUMMARY OF DUAL P-F DROOP METHODS

Method	Advantage	Disadvantage
1	1) Fast-frequency control is solely activated when $\lvert df_{fast} \rvert > df_{th}$ 2) dP_{reg} increases immediately	1) There is a difference between df_{fast} and df_{slow}, leading to a step increase in dP_{reg} 2) dP_{reg} will be calculated as dP_{trans} for few seconds to create a smooth transition from dP_{fast} to dP_{slow}
2	1) Since both fast- and slow-frequency controls are operating, the switching between two control modes does not exist 2) dP_{reg} will always be calculated as the summation of dP_{fast} and dP_{slow}, which makes method 2 a simpler dual *p-f* droop control	1) Both fast- and slow-frequency controls are operating when $\lvert df_{fast} \rvert > df_{th}$ 2) dP_{reg} increases slowly, which is to be investigated in the second case study to prove its insignificance

V. POWER SUPPLY-DEMAND BALANCING (SLOW RESPONSE)

A. Simulation Model

The Institute of Electrical Engineers of Japan (IEEJ) developed a simulation model for frequency regulation called AGC30 [29] which can simulate the supply and demand balance control. This simulation model consists of elements such as conventional power plants, load frequency control (LFC), economic dispatch control (EDC), inertia, tie-line power flow, and time-domain data about the fluctuation of electricity demand and solar irradiance.

In AGC30, two sets of power demand data are prepared with consideration of average characteristics of fluctuations of ten electric power system areas in Japan on the days with a large power demand in the summer season and a small power demand in the spring and autumn seasons. As for the solar irradiance, six sets of time-series data with different weather conditions are prepared.

Figure 8 shows the simulation model of supply-demand frequency. The PV power source with the proposed dual *p-f* droop control is added to the model.

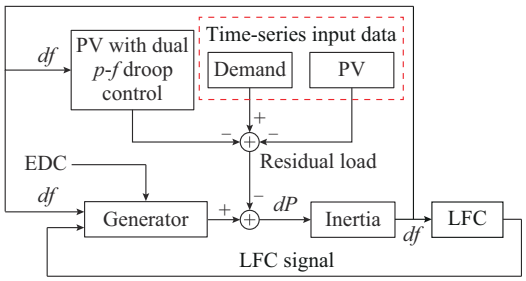

Fig. 8. Simulation model of supply-demand frequency.

Five different patterns of large fluctuations are extracted for different weather conditions during the daytime and used as standard data. Since the solar power output data is usually inaccurate, smoothing effect is considered to remove the influence of local cloud movements. However, it is extremely difficult to measure all the power outputs of many individual solar power plants installed in the area and add them up. Therefore, it is desirable to create the standard data, which are used in this paper since solar power output are multi-point solar radiation data acquired from the Ministry of Economy, Trade, and Industry's subsidized project [29]. In addition, the standard data are the average solar radiation intensity in the area where the smoothing effect is taken into consideration, and the power generation output is calculated by multiplying the assumed installed capacity and the system efficiency.

In the case studies, the semi-clear day pattern time-series data of PV have been prepared by IEEJ [29]. Figure 9 shows the time-series data of demand, residual load, and solar power for 600 s from 10:00 to 10:10 of semi-clear day in summer. The simulation interval of running this model is 0.1 s, which is the same as that of the original AGC30 model.

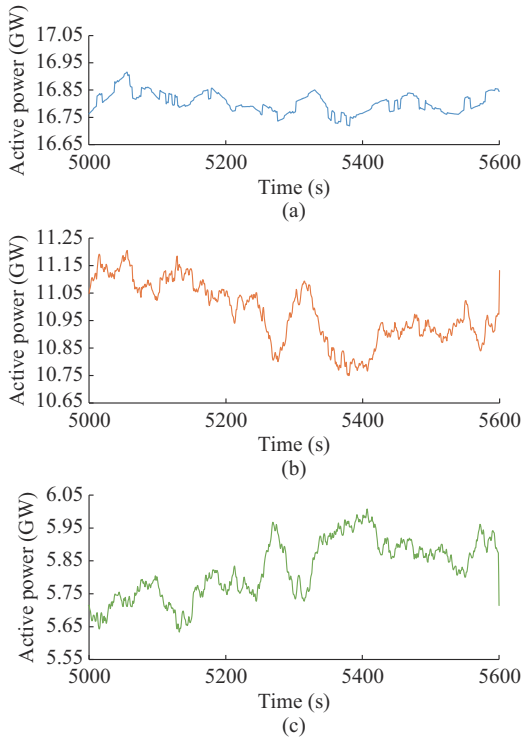

Fig. 9. Time-series data of demand, residual load, and solar power. (a) Demand. (b) Residual load. (c) Solar power.

The transmission system operator (TSO) can set the duration of the power output of aggregated PV system using dual *p-f* droop control. The duration can be for several minutes during certain time of a day. Therefore, the time-series data are almost smooth and steady for this short period. If the irradiance is changed, the time-series data can be obtained at higher or lower steady power output for that short period.

As mentioned above, the proposed control of the PV system is introduced to investigate the contribution of dP_{reg} when the demand and solar input data are fluctuating, assuming the active power of aggregated synchronous generator input is constant.

1) Time-series Data of Demand and PV Output

As shown in Fig. 9, the power demand is almost constant at 16.8 GW with small fluctuations ranging between 16.75

and 16.90 GW. The maximum output data can be obtained from (3). When the maximum solar radiation is 1000 W/m^2, we multiply solar irradiance I by the installed capacity of solar power S and solar power system output coefficient $\eta = 0.8$ to get P_{mpp}, which is the solar data in Fig. 8. The residual load, i. e., P_{mpp} data subtracted from demand data, is shown in Fig. 7.

$$P_{mpp} = \eta S \frac{I}{1000} \tag{3}$$

2) PV Power with Proposed Control

In [31], four strategies of active power curtailment of RES are described. A curtailment approach is among them based on the application of DG production set-points corresponding to a fixed percentage of the actual available power. This measure against high penetration of RES can be easily performed in the most common RES units such as the disconnection of some PV modules. This strategy implicates the largest amount of curtailed energy concerning other solutions. Therefore, this method is generally adopted seasonally, reaching the same performance of the fixed power curtailment.

The capacity of the PV system is 10 GW and the average solar output P_{mpp} is 5800 MW, which is the yield of irradiance. P_{mpp} is curtailed by 20% using the generation of a fixed portion of available production approach [31], thus 4640 MW is available for the proposed control. We assume that 10% of this available power, which accounts for 464 MW, is used for dual *p-f* droop control. Specifically for this amount of PV penetration, only 10% is sufficient to contribute to frequency regulation, whereas the increase in this percentage is expected to cause more violations in the power system. Therefore, the variations in this percentage and its influence on the model can be investigated in future work.

The droop parameter, which determines the *p-f* characteristic of a generating unit, is generally expressed as a percentage [32]. The speed drooping characteristic is obtained by adding a steady-state feedback gain, $1/D$, in the turbine-governor transfer function. The action of droop in a generating unit is to decrease the power reference of the prime mover as the frequency increases. The grid codes of various countries stipulate governor droop settings between 3% and 6%, for all units participating in the system frequency regulation [33]. The droop setting used in the turbine-governor is 4% which is considered to be a typical value of droop setting for thermal generators [34]. The same setting is chosen for the proposed control. Besides, a sensitivity analysis is conducted to observe the response of the dual droop control to variant droop settings from 2% to 16%. The optimum choice of droop setting for this specific penetration amount of PV power and the data obtained in the case studies is 4% since the responses of both fast- and slow-frequency controls are effective and obvious.

3) Inertia and Synchronous Generator Models

Figure S1 in Supplementary Material demonstrates the inertial model with a set of parameters given in Table II, which are previously set by the AGC30 model [29]. They are considered to be a mixture of thermal power generation model. Each one has an inertia ranging from 8 MW/MVA to 11 MW/MVA. Therefore, the chosen inertia is 9 MW/MVA. Figure S2 in Supplementary Material shows the generic governor model but the transfer function of $1/(1+0.2s)$ will be omitted to eliminate any delay in the simulation. In AGC30 model, it is assumed that each generator has the capacity of 1 GW and the capacity of aggregated synchronous generator model is set to be 20 GW, which means that 20 generation units are used.

TABLE II
SETTING VARIABLES OF INERTIA MODEL

Variables	Value
Inertia M	9 MW/MVA
Selected power base S_B	1000 MVA
Load frequency capacity K_L	2 MW/Hz
Nominal frequency f_0	60 Hz
Time increment Δt	0.1 s

4) LFC Model and EDC Signal

The LFC system model in Fig. S3 in Supplementary Material is applied to compensate the supply-demand imbalance by using the frequency deviation and tie-line power flow [14]. The inputs of this model are the actual frequency deviations and the fluctuating demand data. These signals will undergo area requirement (AR) calculation, and then the output will be smoothed. The control signal might have some delay causing the system to be unstable as a result of increasing oscillations. This is often avoided by providing a dead zone to the extent that the system can tolerate it. Also, a proportional-integral (PI) controller is used to eliminate any steady-state deviation. To avoid overshooting, the appropriate values for PI controller parameters are stated in Table III. Then, the signal will follow a ramp rate of 2% per minute, and it is assumed that the majority of used thermal generating units are coal power plants. Afterwards, the LFC signal is fed back to the generator model. Finally, the EDC is considered as a constant signal. The EDC is equivalent to the value of the average residual load (11 GW) divided by the capacity of generators (20 GW), which is 0.55.

TABLE III
SETTING VARIABLES OF LFC MODEL

Type	Variable	Value
AR calculation	Control cycle T_s	5 s
	System constant K	0.1 MW/Hz
AR smoothing	Smoothing factor α	0.30
Dead band	AR dead band width	±10 MW
	Dead band Δf	±0.01 Hz
PI controller	Proportional gain K_P	1.0
	Integral gain K_I	0.003

The chosen LFC ramp rate is 2% per minute, which means that 2% of the generator capacity, which is 400 MW of the synchronous generator per minute, is available to support the LFC. In the first case study when the frequency fluctuation rate is higher than 400 MW/min, the fast-frequency control of dual droop control is able to provide frequency regulation so that the frequency fluctuations are mitigated

when the fluctuations violate the frequency threshold value.

The slow-frequency control is activated within the frequency threshold region to support the LFC and mitigate the small fluctuations further to diminish the chances of higher rates of frequency deviations that cross the threshold and are beyond the region where the LFC can be applied. It is also preferable to always contain the fluctuations in this region, since the fast-frequency control might cause fluctuations by changing the response of generators after being activated.

B. Results and Discussion

Figure 10 shows frequency deviation with and without the proposed dual *p-f* droop control. In all cases, the system frequency fluctuates due to the imbalance in the input data of solar power and demand while the power output of generators is adjusted to compensate for the imbalance.

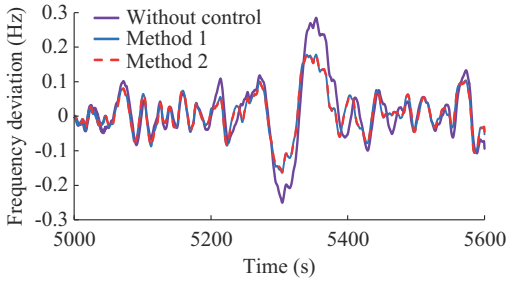

Fig. 10. Frequency deviation with and without proposed dual *p-f* droop control.

Without the proposed dual *p-f* droop control, the maximum frequency deviation reaches 0.284 Hz at 5354 s. Then, the operation of 464 MW of PV power with the proposed dual *p-f* droop control results in further mitigation of the frequency to 0.178 Hz due to the influence of the fast-frequency response of method 1 and method 2. The frequency fluctuations are small within ±0.15 Hz, the fluctuations are generally mitigated by the slow-frequency response of the proposed control. Method 1 and method 2 have almost the same values of frequency deviation, due to their overlapping responses.

1) PV Power Output Deviation of Method 1

In Fig. 11, the application of the proposed control enables the distinction between the frequency measurements due to fast- and slow-frequency responses.

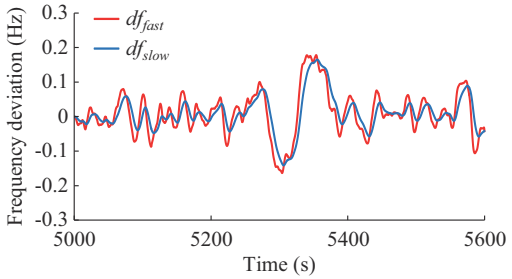

Fig. 11. Measured frequency deviation due to slow- and fast-frequency responses of method 1.

The measured frequency due to fast-frequency response almost follows the actual frequency of the system while the measured frequency due to slow-frequency response has a delay from the actual frequency by a few seconds.

When method 1 of dual *p-f* droop control is implemented in this model, it will result in dP_{reg}, as shown in Fig. 12. dP_{slow} is the output as long as the frequency deviation is within ±0.15 Hz. Once the deviation exceeds ±0.15 Hz, which occasionally happens, dP_{fast} is activated and the new $\pm df_{th}$ becomes ±0.1 Hz. Therefore, dP_{fast} will have an output from the time when it exceeds ±0.15 Hz until the frequency reaches the new threshold of ±0.1 Hz.

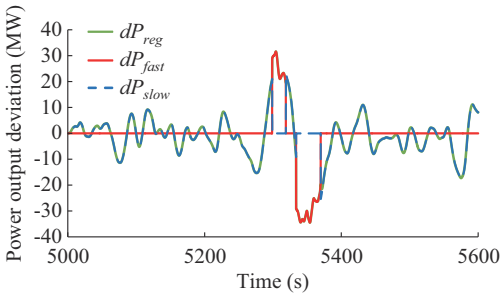

Fig. 12. PV power output deviation due to slow- and fast-frequency responses applying method 1.

The maximum frequency deviation of 0.178 Hz at 5354 s will lead to a maximum power deviation of −34.4 MW due to the activation of fast-frequency response only. The reduction below the threshold point of ±0.1 Hz will enable slow-frequency response again and only dP_{slow} contributes to the output. It is also observed that at the frequency recovery phase, when switching between fast- and slow-frequency modes occur in Fig. 13, dP_{reg} is no longer equal to the sum of dP_{slow} and dP_{fast}. However, it is the yield of the dP_{trans} where dP_{fast} will change to dP_{slow} as stated in Section II for only 3 s. During this period, dP_{reg} increases slightly from −19.6 MW to −21.4 MW instead of −25.4 MW if no transition signal is introduced. After 3 s, dP_{reg} is calculated as the sum of dP_{slow} and dP_{fast} again.

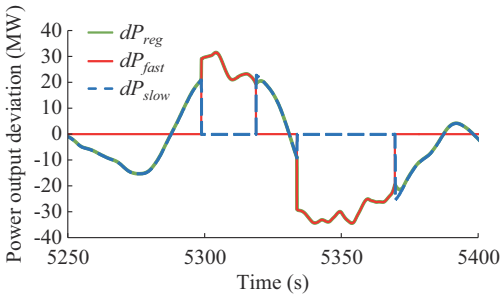

Fig. 13. Magnified PV power output deviation due to slow- and fast-frequency responses applying method 1.

2) PV Power Output Deviation of Method 2

Figure 14 shows PV power output deviation due to slow- and fast-frequency responses applying method 2. In Fig. 15, when $\pm df$ is within ±0.1 Hz, dP_{reg} will be a result of slow-frequency response. Once the frequency crosses the threshold of 0.1 Hz, both the fast- and slow-frequency responses will be activated so the maximum power deviation is −34.4 MW at 5354 s. Method 2 is proposed to prevent the switching of PV power outputs between slow- and fast-frequency

responses and eliminates the time detection used for the transition mode signal at the recovery period. Thus, dP_{reg} is always expressed in terms of the sum of both dP_{slow} and dP_{fast}. Accordingly, when the frequency recovers, dP_{reg} shows a gradual decrease to −19.33 MW at 5370 s due to the influence of slow-frequency response when it operates simultaneously with fast-frequency response. The power outputs due to the slow- and fast-frequency responses of method 1 and method 2 in Fig. S4 in Supplementary Material, and the total regulation power of method 1 and method 2 in Fig. S5 in Supplementary Material, respectively.

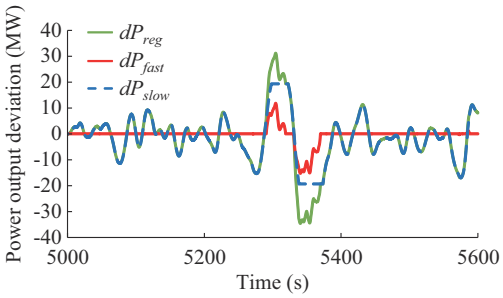

Fig. 14. PV power output deviation due to slow- and fast-frequency responses applying method 2.

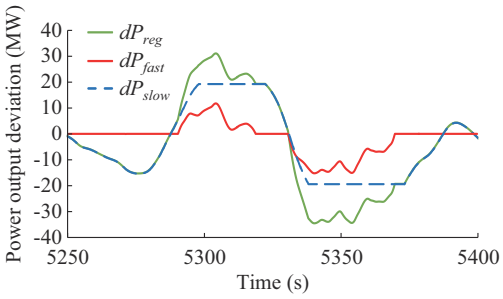

Fig. 15. Magnified PV power output deviation due to slow- and fast-frequency responses applying method 2.

3) Discussion

When comparing the total power deviation results of both methods of dual *p-f* droop control in both phases of normal and abnormal grid frequency deviations, some important conclusions are drawn.

When the demand fluctuations lead to small fluctuations of frequency within $\pm df_{th}$, slow-frequency responses of method 1 and method 2 mitigate the fluctuations generally in that region compared with the case without control. However, frequency fluctuations violate the df_{th} and increase beyond it occasionally. Fast-frequency response of method 1 and method 2 will suppress the fluctuations, and this happens when the load fluctuations are large. Overall, both methods of dual *p-f* droop controls are efficient for mitigating the fluctuations. The transition between the slow- and fast-frequency controls of both methods is depicted through PV power output when each one is applied.

At the recovery phase, when the frequency deviation decreases below df_{th}, method 2 shows a gradual decrease of dP_{reg} while method 1 experiences a slight increase due to the transition mode signal. The simpler approach of method 2 has eliminated the detection of the time for an extra signal application like method 1. As a result, method 2 has proven its simplicity and flexibility when it comes to frequency recovery.

However, power output has a quicker increase in dP_{reg} than method 2 in an abnormal situation. This is caused by the sole operation of fast-frequency response in method 1 in an abnormal situation whereas both slow- and fast-frequency responses occur simultaneously in method 2, which slows down the operation of method 2 at that phase. The slightly delayed response of method 2 in abnormal situations leads to conduct another simulation that detects whether such delay is significant or not.

C. Influence of Slow Response in Dual p-f Droop Control

Referring to Fig. 16, at the infrequent incidents of violating df_{th}, only fast-frequency response will reduce the frequency deviation to 0.182 Hz. As stated previously, method 2 further mitigates the frequency deviation to 0.178 Hz.

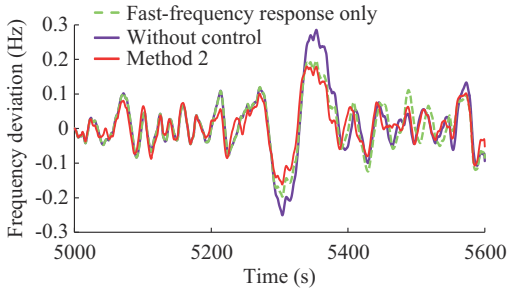

Fig. 16. Frequency deviation due to fast-frequency response only and with dual *p-f* droop control of method 2.

After 5380 s, the occasional mitigation of frequency by the fast-frequency response generates higher variations in frequency following that mitigation. These variations are even more than the case without control. That is because the operation of the thermal generator has changed after that mitigation by fast-frequency response, hence the frequency fluctuation becomes different and larger than the case without control.

This negative effect is suppressed by slow-frequency response using method 2 to witness a lower frequency deviation, emphasizing the importance of slow-frequency response. This affirms the idea that slow-frequency response working along with the fast-frequency response can maintain the frequency deviation at a lower level.

VI. Effect on Inertial Support (Fast Response)

A. Simulation Model

The model in Fig. 17 illustrates a simplified model of AGC30 that involves the same components as the previous test model without using LFC, which makes this test model concern the primary frequency response only. The simulation time interval is 0.01 s to realize the sudden incident of generator tripping and frequency drop.

The proposed control is tested when the generator trips and it is assumed that demand and solar input data are constant in this scenario. The constant demand is rated to be

16.8 GW. The capacity of the PV is 10 GW and the power utilized by the dual *p-f* droop control is equivalent to 464 MW. The droop setting of the dual *p-f* droop control is also 4%. These are the same assumptions as considered in the previous test.

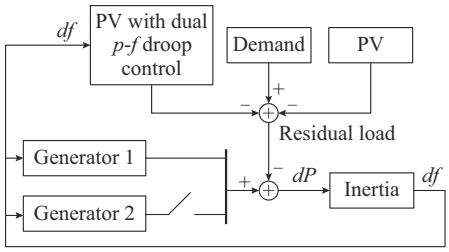

Fig. 17. Simplified model of AGC30 without using LFC.

The settings of parameters of the inertial model are the same as those shown in Table II. Both generators in the model have a total capacity of 20 GW. The capacity of generator 2 corresponds to 5% of the overall capacity which is equivalent to 1 GW in this test. The generator model is slightly different from that used in the previous model because when the generator trips, we have to observe a few seconds that immediately follow this drop. Accordingly, the generic model of the turbine governor will be used without the omission of the transfer function to observe the reaction of the frequency in a shorter time interval and distinguish the influence of dual *p-f* droop control. In this model, the frequency is not restored to its nominal value of 60 Hz due to the absence of the LFC system.

B. Results and Discussion

In Fig. 18, without implementing the proposed control, which emulates the test of free-governor control only, the frequency deviation of the system will drop to –0.435 Hz and the frequency is recovered to a deviation of –0.162 Hz due to the absence of the LFC. While the mere application of slow-frequency control results in a frequency deviation of –0.397 Hz and recovers to –0.117 Hz quicker than the proposed control. The power due to slow-frequency response will be higher since the slow-frequency measurement is slightly delayed. Therefore, it detects higher frequency change.

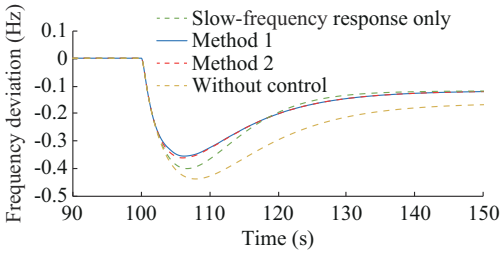

Fig. 18. Frequency deviation response in absence of LFC system.

When dual *p-f* droop control is implemented, the frequency deviation is mitigated to –0.353 Hz and –0.360 Hz by method 1 and method 2, respectively, and it is recovered to –0.117 Hz. It is also observed that the frequency deviation values of both methods are almost the same, which leads to the values overlapping from 115 s.

1) PV Power Output Deviation of Method 1

Fast-frequency response of method 1 causes regulation power to increase steeply to 71 MW, as shown in Fig. 19. Regulation power due to fast-frequency response is supposed to stop when it hits df_{th} of –0.15 Hz. However, regulation power continues till df_{th} of –0.1 Hz, which is the new value of df_{th}, following the characteristics of method 1. The power starts to decrease, hitting the peak when the largest frequency occurs. Contrarily, due to the slow-manner of frequency detection of slow-frequency control, it will still be activated even though *df* is less than –0.1 Hz (df_{th}), resulting in a significant power increase in dP_{reg}. It reaches 544 MW. Eventually, the power due to slow-frequency response will drop to zero power deviation that will lead to a slightly steep decrease in dP_{reg} as shown in Fig. 20.

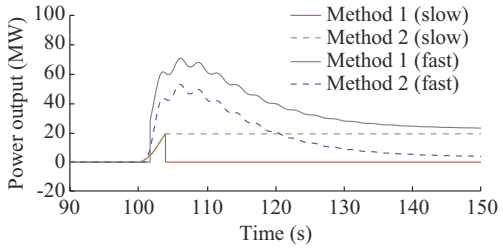

Fig. 19. PV regulation power output due to slow- and fast-frequency responses of method 1 and method 2.

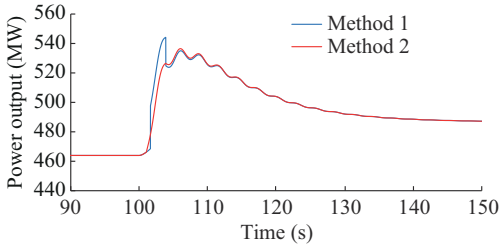

Fig. 20. Total PV regulation power output applying method 1 and method 2.

2) PV Power Output Deviation of Method 2

The application of method 2 of dual *p-f* droop control has shown that power output due to fast-frequency response in Fig. 19 will increase to 53 MW. Regulation power due to slow-frequency response is provided when *df* decreases below –0.1 Hz. Fast- and slow-frequency responses will operate concurrently beyond df_{th} which results in the fact that dP_{reg} is the sum of power due to fast- and slow-frequency responses equivalent to 536 MW. As a result, dP_{reg} in method 2 in Fig. 20 seems to have a smoother increase than that in method 1. Then, the supply of dP_{reg} due to both methods almost overlaps since the droop settings used in both methods are the same.

3) Discussion

The maximum frequency deviation is realized when no control is applied which simulates the condition of the inertial response of the existing generator. When the slow-response suppresses the frequency deviations, it is further sup-

pressed by the proposed control due to the activation of the fast-frequency response. The positive influence of fast-frequency response in the proposed control confirms a rapid recovery and further a reduction in frequency deviation.

There is a slight difference between frequency deviation due to the application of method 1 and method 2 at 103 s. The reason is that the activation of only fast-frequency response in method 1 and the simultaneous operation of slow-frequency response along with fast-frequency response in method 2 in abnormal operation state delays the quick action of fast-frequency response to be marginally slower than that of method 1. However, this slight difference is considered insignificant since method 2 still has a quicker reaction compared with the inertia of the generator in the system without the proposed control.

Moreover, the results of dP_{reg} have revealed a surge of power output when using method 1 due to the switching from fast- to slow-frequency responses. Therefore, the proposal of a simple control scheme such as method 2 proves a smooth PV power output due to the operation of slow- and fast-frequency responses, simultaneously.

4) Validation of Results

In [21], PV droop control is applied in the form of an FW curve where the active power is changed according to the frequency. That is to deploy distributed APC that provides ancillary services including regulation and primary contingency reserves. It also investigates the influence of multiple parameters of FW function on the performance of a small island grid. In this paper, FW function is nearly equivalent to the fast-frequency control of the proposed control. FW function is tested with different scenarios of PV penetrations depending on the number of online generators. Moreover, various ranges of PV power curtailment, dead band and droop setting of FW control are tested [21]. One of the tests is conducted using 70% PV penetration, and the incident is the loss of one out of three diesel generators. Also, the dead band is ±0.1 Hz, and the droop setting is 0.0125 Hz. The results of generator frequency in the cases of 50% curtailment (without frequency support case) and FW response of PV power are presented in [21]. The contribution of FW response is obvious through mitigating the frequency as in fast-frequency control, when the dead band crosses −0.1 Hz more than the case without FW function support.

In the proposed control, fast-frequency control has approved the same concept of results, when the scenario of generation loss happens, i. e., the frequency deviations are further mitigated compared with the case with merely PV curtailment. Besides, droop control can accommodate different frequency control characteristics, in particular slow- and fast-frequency responses to form a dual *p-f* droop control. The significance of slow-frequency control is demonstrated in the scenario of load fluctuations where the frequency fluctuations are further mitigated even before crossing the dead band. Therefore, slow-frequency response can suppress the fluctuations so that they hardly violate the dead band. Finally, the effectiveness of the proposed control is highlighted in two main scenarios to signify the slow- and fast-frequency controls, respectively.

Another study case similar to that in Section V is conducted to investigate the effectiveness of the proposed control when increasing frequency deviation. It is implemented by reducing the demand power, so the power of the generators rises accordingly. The frequency deviation for applying the proposed control is less than that without control, as shown in Fig. 21.

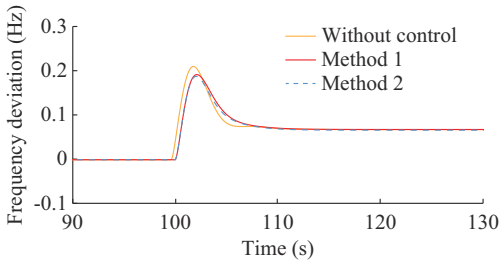

Fig. 21. Frequency deviation response due to load reduction.

Another aspect is concluded after running this test, which is the duration of frequency saturation. In both cases, the saturation time is after 20 s after the incident, whereas 50 s is the saturation time when the generators' power is changed as shown in Fig. 21. In the case of demand power reduction, a faster saturation time is expected since the governor power is sustained and only the loads increase, which makes the generator overcome this incident quickly. However, in the case of generation loss, it takes a longer time for the generator to overcome the loss and suppress the frequency deviation.

VII. Conclusion

Autonomous APC for supporting LFC and the inertial response of synchronous generators is proposed by creating two different characteristics for slow- and fast-frequency dynamic responses provided by small-scale PV systems. Two simple control methods of dual *p-f* droop control are designed to achieve a smooth transition between slow- to fast-frequency responses according to the change in frequency.

Two simulation models are conducted to highlight the importance of slow- and fast-frequency responses of both methods. The results reveal that the slow- and fast-frequency controls can work independently to eliminate the negative influence of each another. The switching between slow- and fast-frequency controls in emergency and recovery phases has shown that method 2 of the proposed control provides smoother transitions than method 1. This proves that method 2 outperforms method 1 as an effective control for supporting frequency by small-scale PV systems.

As future work, the authors are going to consider an adaptive droop setting for the proposed approach, concerning the dynamic of frequency deviation and the rate of PV power generation. Then, a sensitivity analysis will be also done for some factors such as the used frequency threshold, and the degree of changing the PV power experiencing dual *p-f* droop control. Accordingly, the impact of this variability on the system frequency deviation will be investigated. Finally,

various changes in demand data especially their surge will reflect the future inflation of demand, thus the effectiveness of the proposed control under this condition should be tested.

Developing an adaptive droop setting is considered as the future step of the present work. For example, in the case of slow-frequency control, the same value of droop setting can be used. And in fast control, higher value of droop setting can be decided to give a quicker response and mitigate the frequency deviations. Moreover, for every penetration amount of PV power, an optimum value of droop setting can be chosen.

REFERENCES

[1] K. Y. Yap, C. R. Sarimuthu, and J. M. Y. Lim, "Artificial intelligence based MPPT techniques for solar power system: a review," *Journal of Modern Power Systems and Clean Energy*, vol. 8, no. 6, pp. 1043-1059, Nov. 2020.

[2] M. A. G. de Brito, L. Galotto, L. P. Sampaio *et al.*, "Evaluation of the main MPPT techniques for photovoltaic applications," *IEEE Transactions on Industrial Electronics*, vol. 60, no. 3, pp. 1156-1167, Mar. 2013.

[3] B. Subudhi and R. Pradhan, "A comparative study on maximum power point tracking techniques for photovoltaic power systems," *IEEE Transactions on Sustainable Energy*, vol. 4, no. 1, pp. 89-98, Jan. 2013.

[4] R. Golden and B. Paulos, "Curtailment of renewable energy in California and beyond," *The Electricity Journal*, vol. 28, no. 6, pp. 36-50, Jun. 2015.

[5] D. Lew, L. Bird, M. Milligan *et al*., "Wind and solar curtailment," in *Proceedings of the Conference Proceedings 12th International Workshop on Large-scale Integration of Wind Power into Power Systems as well as on Transmission Networks for Offshore Wind Power Plants*, London, UK, Sept. 2013, pp. 1-6.

[6] R. Luthander, D. Lingfors, and J. Widén, "Large-scale integration of photovoltaic power in a distribution grid using power curtailment and energy storage," *Solar Energy*, vol. 155, pp. 1319-1325, Nov. 2017.

[7] X. Su, M. A. S. Masoum, and P. J. Wolfs, "Optimal PV inverter reactive power control and real power curtailment to improve performance of unbalanced four-wire LV distribution networks," *IEEE Transactions on Sustainable Energy*, vol. 5, no. 3, pp. 967-977, Jul. 2014.

[8] Network Code. (2013, Mar.). Network code for requirements for grid connection applicable to all generators. [Online]. Available: https://www.entsoe.eu/network_codes/rfg/

[9] Regulations for Grid Connection. (2016, Jun.). Technical regulation 3.2.2 for PV power plants above 11 kW. [Online]. Available: https://en.energinet.dk/Electricity/Rules-and-Regulations/Regulations-for-grid-connection

[10] A. Howlader, S. Sadoyama, L. Roose *et al.*, "Active power control to mitigate voltage and frequency deviations for the smart grid using smart PV inverters," *Applied Energy*, vol. 258, p. 114000, Sept. 2020.

[11] H. Bevrani, *Robust Power System Frequency Control*. New York: Springer, 2014.

[12] H. Bevrani and T. Hyama, *Intelligent Automatic Generation Control*. New York: CRC Press, 2017.

[13] V. Gevorgian and B. O'Neill, "Advanced grid-friendly controls demonstration project for utility-scale PV power plant," United States, Tech. Rep. NREL/TP-5D00-65368, Jan. 2016

[14] Q. Hong, M. Nedd, S. Norris *et al*., "Fast frequency response for effective frequency control in power systems with low inertia," *The Journal of Engineering*, vol. 2019, no. 16, pp. 1696-1702, Oct. 2018.

[15] W. Bo, S. Chong, S. Weichneng *et al.*, "Actual measurement and analysis of wind power plant participating in power grid fast frequency modulation base on droop characteristic," in *Proceedings of International Conference on Power System Technology*, Guangzhou, China, Jul. 2018, pp. 1552-1557.

[16] J. Morren, S. W. H. de Haan, W. L. Kling *et al*., "Wind turbines emulating inertia and supporting primary frequency control," *IEEE Transactions on Power Systems*, vol. 21, no. 1, pp. 433-434, Feb. 2006.

[17] P. Yang, X. Dong, Y. Li *et al*., "Research on primary frequency regulation control strategy of wind-thermal power coordination," *IEEE Access*, vol. 7, pp. 144766-144776, Oct. 2019.

[18] Y. Wang, H. Bayem, M. Giralt-Devant *et al*., "Methods for assessing available wind primary power reserve," *IEEE Transactions on Sustainable Energy*, vol. 6, no. 1, pp. 272-280, Dec. 2014.

[19] R. K. Varma and M. Akbari, "Simultaneous fast frequency control and power oscillation damping by utilizing PV solar system as PV-STATCOM," *IEEE Transactions on Sustainable Energy*, vol. 11, no. 1, pp. 415-425, Jan. 2020.

[20] C. Loutan, P. Klauer, S. Chowdhury *et al*., "Demonstration of essential reliability services by a 300-MW solar photovoltaic power plant," USA, Tech. Rep. TP-5D00-67799, Mar. 2017.

[21] J. Johnson, J. C. Neely, J. J. Delhotal *et al*., "Photovoltaic frequency-watt curve design for frequency regulation and fast contingency reserves," *IEEE Journal of Photovoltaics*, vol. 6, no. 6, pp. 1611-1618, Nov. 2016.

[22] H. Xin, Y. Liu, Z. Wang *et al.*, "A new frequency regulation strategy for photovoltaic systems without energy storage," *IEEE Transactions on Sustainable Energy*, vol. 4, no. 4, pp. 985-993, Oct. 2013.

[23] A. F. Hoke, M. Shirazi, S. Chakraborty *et al*., "Rapid active power control of photovoltaic systems for grid frequency support," *IEEE Journal of Emerging and Selected Topics in Power Electronics*, vol. 5, no. 3, pp. 1154-1163, Sept. 2017.

[24] J. Neely, J. Johnson, J. Delhotal *et al.*, "Evaluation of PV frequency-watt function for fast frequency reserves," in *Proceedings of IEEE Applied Power Electronics Conference and Exposition (APEC)*, Long Beach, USA, Jun. 2016, pp. 1926-1933.

[25] C. S. Psomopoulos, G. C. Ioannidis, and S. D. Kaminaris, "Electricity production from small-scale photovoltaics in urban areas," in *Renewable and Alternative Energy: Concepts, Methodologies, Tools, and Applications*, Madrid: Information Resources Management Association, IGI Global, Jan. 2017.

[26] A. B. Eltantawy and M. M. A. Salama, "Management scheme for increasing the connectivity of small-scale renewable DG," *IEEE Transactions on Sustainable Energy*, vol. 5, no. 4, pp. 1108-1115, Oct. 2014.

[27] S. Cobben, B. Gaiddon, and H. Laukamp. (2008, Nov.). Impact of photovoltaic generation on power quality in urban areas with high PV population. [Online]. Available: https://www. acdemia. edu/1439223/IMPACT_OF_PHOTOVOLTAIC_GENERATI N_ON_POWER_QUALITY_IN_URBAN_AREAS_WITH_HIGH_PV_POPULATION_Results_from_Monitoring_Campaigns

[28] C. A. Christodoulou, N. P. Papanikolaou, and I. F. Gonos, "Design of three-phase autonomous PV residential systems with improved power quality," *IEEE Transactions on Sustainable Energy*, vol. 5, no. 4, pp. 1027-1035, Oct. 2014.

[29] IEEJ, "Recommended practice for simulation models for automatic generation control," Japan. Tech. Rep. Dec. 2016.

[30] Organization for Cross-regional Coordination of Transmission Operators. (2018, Nov.). Report on the quality of electricity supply. [Online]. Available: https://www.occto.or.jp/en/information_disclosure/miscellaneous/files/170203_qualityofelectricity.pdf

[31] M. Rossi, G. Viganò, D. Moneta *et al*., "Analysis of active power curtailment strategies for renewable distributed generation," in *Proceedings of 2016 AEIT International Annual Conference (AEIT)*, Capri, Italy, Oct. 2016, pp. 1-6.

[32] P. Kundur, *Power System Stability and Control*. New York: McGraw-Hill, Inc., 1994.

[33] K. V. Vidyanandan and N. Senroy, "Primary frequency regulation by deloaded wind turbines using variable droop," *IEEE Transactions on Power Systems*, vol. 28, no. 2, pp. 837-846, May 2013.

[34] R. E. Cosse, M. D. Alford, M. Hajiaghajani *et al.*, "Turbine/generator governor droop/isochronous fundamentals – a graphical approach," in *Proceedings of 2011 Record of Conference Papers Industry Applications Society 58th Annual IEEE Petroleum and Chemical Industry Conference (PCIC)*, Toronto, Canada, Aug. 2011, pp. 1-8.

[35] K. D. Brabandere, B. Bolsens, J. V. den Keybus *et al*., "A voltage and frequency droop control method for parallel inverters," *IEEE Transactions on Power Electronics*, vol. 22, no. 4, pp. 1107-1115, Jul. 2007.

[36] J. M. Guerrero, L. G. de Vicuna, J. Matas *et al*., "A wireless controller to enhance dynamic performance of parallel inverters in distributed generation systems," *IEEE Transactions on Power Electronics*, vol. 19, no. 5, pp. 1205-1213, Sept. 2004.

Noha Harag received the B. Sc. degree in renewable energy engineering from University of Science and Technology, Zewail City, Egypt, in 2018, and the M.Sc. degree in electrical engineering from Nagoya University, Nagoya, Japan, in 2020. She is currently pursuing her Ph.D. degree in electrical engineering from Nagoya University. Her research interests include control solutions to integrated energy systems and power system dynamics.

Masaki Imanaka received the B. Sc. degree in electrical engineering in 2010, and M.Sc. and Ph.D. degrees in 2012 and 2015, respectively, in advanced energy from the University of Tokyo, Tokyo, Japan. He is currently an Assistant Professor of Nagoya University, Nagoya, Japan. His research interests include renewable energy sources, load control, distribution network, and island power.

Muneaki Kurimoto received the B.Sc. degree in 2001, the M.Sc. degree in 2003, and the Ph.D. degree in 2010, all in electrical engineering, from Nagoya University, Nagoya, Japan. From 2003 to 2007, he joined Aisin Seiki Corporation, Nagoya, Japan. From 2010 to 2013, he was an Assistant Professor at Toyohashi University of Technology, Toyohashi, Japan. Since 2018, he has been an Associate Professor at Nagoya University. His research interests include nanocomposite dielectrics for high efficiency power apparatus and systems.

Shigeyuki Sugimoto received the B.Sc. degree in 1981, the M.Sc. degree in 1983, and the Ph.D. degree in 1999, all in electrical engineering, from Gifu University, Gifu, Japan. From 1983 to 1991, he joined Nagoya Works, Mitsubishi Electric Co., Ltd., Nagoya, Japan. Since 1991, he has been with Electric Power R&D Center, Chubu Electric Power Co., Inc., Nagoya, Japan. He has also been a Designated Professor at Nagoya University since 2018. His research interests include power systems applying power electronics technologies.

Hassan Bevrani received the Ph. D. degree in electrical engineering from Osaka University, Suita, Japan, in 2004. He is currently a Full Professor and the Program Leader with the Smart/Micro Grids Research Center, University of Kurdistan, Sanandaj, Iran. His research interests include smart grid operation and control, power system stability and optimization, microgrid dynamics and control, and intelligent/robust control applications in power electric industry.

Takeyoshi Kato received the B. Sc. degree in 1991, the M. Sc. degree in 1993, and the Ph.D. degree in 1996, all in electrical engineering, from Nagoya University, Nagoya, Japan. From 1996 to 2015, he was on the faculty of Nagoya University. Since 2015, he has been a Professor at Nagoya University. His research interests include modeling/forecasting of electricity demand and renewable power output, control and planning of electric power system, and integration of renewable energy with urban design.